On the optimal choice of fibre orientation angle in off-axis tensile test using oblique end-tabs: theoretical and experimental studies.

J.C. Marín, J. Justo, A. Barroso, J. Cañas, and F. París

E.T.S. Ingeniería, Universidad de Sevilla, Camino de los Descubrimientos s/n, 41092 Sevilla, Spain

Abstract

Shear strength evaluation in composite materials still remains a not fully solved problem. One of most promising proposals to characterize a material in shear by means of a simple tensile test is the off-axis tension test with oblique end-tabs whose inclination coincides with that of the longitudinal isodisplacement lines. This end-tab configuration presents an essential difficulty since the tab angle depends on the material properties including the shear modulus G_{12}, which is one of the values to be obtained from off-axis tension tests.

In the present work, the study of the most suitable fibre orientation for the performance of off-axis tests under an oblique tabs configuration has been addressed. An analytical study on the dependence of the tab angle ϕ on both the fibre orientation θ and the material properties E_{11}, E_{22}, ν_{12} and G_{12} has been carried out, the quotient G_{12}/E_{11} being identified as the parameter that controls the evolution of the tab angle.

The influence of deviations in the tab angle on the stress state near the corners of specimen has been analysed by means of a novel study of the nominal singular stress state at these points. The results of this study show that negative deviations in the angle of the tabs contribute to decrease the severity of the stress state at the corner, whereas positive deviations contribute to increase the order of the stress singularity.

Additionally, the range of fibre orientations in which the evaluation of shear strength S

is feasible has been determined, i.e., the effect of σ_{12} in the failure is clearly dominant versus the effect of the rest of the stress-state components.

In the experimental part of this work, four different fibre orientation angles (5º, 10º, 15º and 20º) have been considered to perform the off-axis tension test under oblique end-tabs configuration. The experimental results of these tests show that only for 10º fibre orientation angle the majority of specimens fail at the central zone under a uniform stress state. Finally, for a fibre orientation angle $\theta = 10º$, specimens with induced positive deviations in tab angle of +3º and +7º have been tested, it being observed that all the failures appears at the end of specimens.

On the basis of both theoretic and experimental results, the optimal fibre orientation angle to use in the tests is $\theta = 10º$. The tab angle must be evaluated on the basis of an estimation of the material properties (quotient G_{12}/E_{11}), it being recommendable, in case of ignoring the value of G_{12}, to use a tab angle lesser than the theoretical value to avoid positive deviations.

Keywords: B. Shear strength; D. Off-axis tensile test; C. Stress concentrations.

1. Introduction

Shear characterization of unidirectional layers for composite materials continues being a not fully solved problem. In the last fifty years many different approaches have been proposed to solve this problem (rail shear test [1-7], thin-walled tube torsion test [8, 9], off-axis tensile test [10-22], ±45º tensile test [23-26], Arcan test [27-30], Iosipescu test [31-33], asymmetric four-point bend test [34, 35], plate twist test [36, 37], v-notched rail shear test [38-40], off-axis flexural test [41-43] and shear frame test [44]), although anyone of these approaches has achieved an unquestionable support. In general, a characterization test must be as simple as a tensile test, and mainly for this reason, the

most successful approach for shear characterization has been the ±45º tension test [23]. Although is notorious [26] that the strength value obtained from this test is not the intralaminar shear strength S, because the ±45º layers fail due to a dominant normal transversal stress component σ_{22}.

One of most common tests for composite materials is the off-axis tension test. This test is frequently used in shear characterization of unidirectional layer specimens and in the study of the off-axis behaviour of different fibre orientation angles under both static and fatigue loads. However, it is well known that the difficulties in the experimental performance of off-axis tension tests are associated with the coupling effect (Pagano & Halpin [10]). Two types of approaches have been proposed to solve these difficulties: the application of correction factors to the direct measurement of the test (Pindera & Herakovich [17], Marín et al [21]), and the modification of the test fixture to attain a situation that best approximates a pure tension stress field. For the latter, several different approaches have been proposed (Pindera & Herakovich [17], Cron et al. [18], Sun & Berreth [19], Sun & Chung [20], Xiao et al. [22]). Among these studies, the approach proposed by Sun & Chung [20] has achieved a certain remarkable relevance. This approach involves the use of oblique end-tabs whose angle agrees with isodisplacement lines for an ideal test configuration. Pierron & Vautrin [45] have shown, by numerical study (finite element method (FEM)) of a 10-degree off-axis configuration, that specimens with oblique end-tabs present a more uniform stress field than specimens with regular end-tabs. Additionally, the stress concentration that appears at the corners of the specimen can be reduced by using an oblique end-tab configuration. This fact, which was experimentally verified by Kawai et al. [46] by means of strain gages and by Pierron et al. [47] by means of a grid technique, constitutes the great advantage that this configuration has in connection with strength characterization. Nevertheless, as pointed out by Pierron & Vautrin [45], the oblique

end-tab configuration does not produce a pure shear stress field; hence, a failure criterion is needed to evaluate in-plane shear strength S. The same authors, in a later work [48], show that coherent values of S can be obtained by applying the Tsai-Wu criterion to the results of both a 10-degree off-axis tension test and a 0-degree Iosipescu test for the same material.

However, the oblique end-tab configuration presents an essential difficulty. The angle of the tabs ϕ depends on the material properties including the shear modulus G_{12}, which is one of the values that is determined from off-axis tension tests. Pierron et al. [47], by means of a sensitivity analysis, show that the most influential parameters for the angle of the tabs are E_{11} and G_{12}. Additionally, based on numerical results (FEM) for a 10-degree fibre orientation angle, they concluded that a difference of 3 degrees in the oblique angle resulted in non-significant stress concentrations near the tabs; however, a difference of 7 degrees can lead to significant stress concentrations near the tabs.

In the present work, the most adequate fibre orientation angle to perform an off-axis tensile test under an oblique end-tabs configuration is theoretically and experimentally studied; this orientation angle should meet the following three conditions:

- The associated oblique angle of the tabs should present as little variation as possible with material properties.
- The fibre orientation should be adequate for shear modulus evaluation G_{12}.
- The fibre orientation should be adequate for shear strength evaluation S.

To consider the first condition, an analytical study has been performed regarding the variation in the angle of the oblique end-tab ϕ with the fibre orientation θ and material properties E_{11}, E_{22}, ν_{12} and G_{12}. The second condition is not as restrictive as the others,

because accurate G_{12} values can be obtained by different fibre orientation angles from 10º to 45º. Former studies have proved that the optimal orientation to produce maximum values of γ_{12} is around 10 degrees (Chamis & Sinclair [15]). To consider the last condition, a novel study of the singularities of the nominal stress state at the corner, to evaluate the changes in stress state at the ends of a specimen due to deviations in the tab angles, has been carried out. Additionally, the adequate orientation interval to evaluate shear strength S has been determined. Several failure criteria have been employed for this purpose.

Then, to support the theoretical results, a campaign of off-axis tensile tests under oblique tab configuration has been carried out. Different fibre orientations have been considered (5º, 10º, 15º and 20º) in these tests. The corresponding tab angles for these orientations have been estimated in the basis of the manufacturer's values of material properties. The experimental results and the failures observed for the different orientations have been considered separately.

2. Oblique end-tab setup for off-axis tension tests.

The nominal off-axis tension test configuration consists of a rectangular unidirectional layer specimen whose fibres are oriented at an angle θ with respect to the longitudinal direction x, as shown in figure 1(a). This unidirectional layer specimen is ideally subjected to a uniform distribution of longitudinal stress $\sigma_x = \sigma$. Under these boundary conditions, the lines of longitudinal isodisplacement are straight lines that lie at an angle ϕ with respect to the x-axis; this angle can be derived from the analytical solution of the problem, and it can be expressed as [20]:

$$\cot\phi = -\frac{\bar{S}_{16}}{\bar{S}_{11}}, \tag{1}$$

where $\bar{S}_{11}$ and $\bar{S}_{16}$ are the compliance coefficients. These compliance coefficients can be evaluated as follows:

$$\begin{aligned}\bar{S}_{11} &= \frac{\cos^4\theta}{E_{11}} + \left(-\frac{2\nu_{12}}{E_{11}} + \frac{1}{G_{12}}\right)\sin^2\theta\cos^2\theta + \frac{\sin^4\theta}{E_{22}} \\ \bar{S}_{16} &= \left(\frac{2}{E_{11}} + \frac{2\nu_{12}}{E_{11}} - \frac{1}{G_{12}}\right)\sin\theta\cos^3\theta + \left(-\frac{2\nu_{12}}{E_{11}} - \frac{2}{E_{22}} + \frac{1}{G_{12}}\right)\sin^3\theta\cos\theta\end{aligned}. \tag{2}$$

Sun & Chung [20] propose the use of oblique end-tabs with an angle ϕ (figure 1(b)), which produces a constant displacement along the lines of longitudinal isodisplacement at the ends of the specimen.

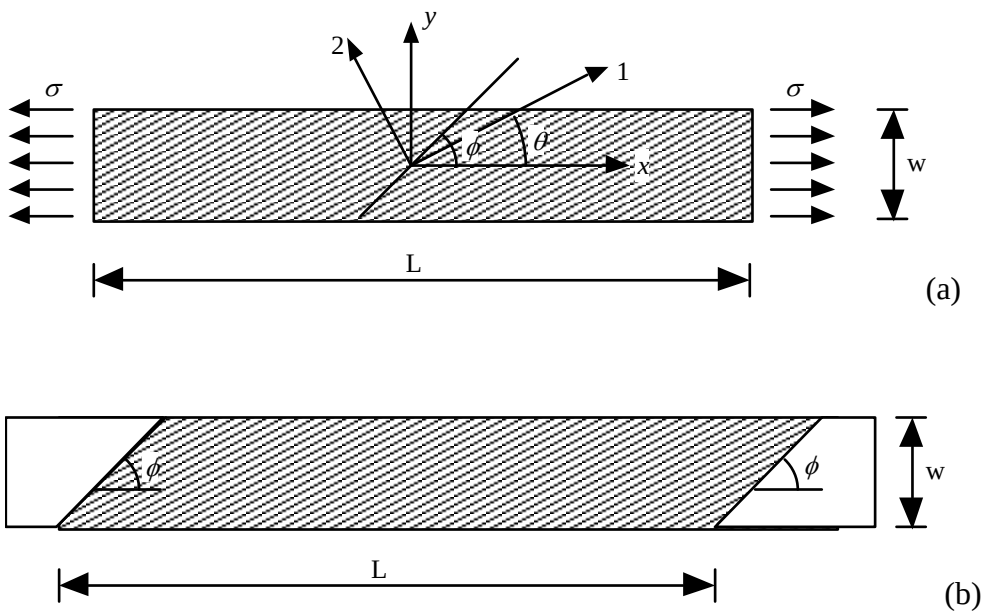

Figure 1. (a) Nominal off-axis tension test configuration. (b) Oblique end-tab specimen.

Equations (1) and (2) indicate that the angle of the end-tab ϕ depends on both material properties (E_{11}, E_{22}, G_{12} and ν_{12}) and fibre orientation angle θ. The fibre orientation angle is known before the specimen manufacturing, but the material properties are generally unknown. Therefore, the practical performance of a test requires a previous assumption regarding the material property values. Obviously, the validity of the G_{12} and S values obtained from this test depends on the validity of the assumption realized regarding the material property values. The feasibility of the testing procedure would thus be constrained by the sensitivity of the tab angle ϕ to variations in material properties.

3. Study of the tab angle ϕ as a function of material properties.

Given the great diversity of properties (E_{11}, E_{22}, G_{12} and ν_{12}) in composite materials, it seems unlikely that a unique tab angle could be found to be adequate for all materials. However, it is reasonable to find a unique orientation of tabs that is applicable to one material type, generating acceptable errors in the evaluation of G_{12} and S. The properties for graphite-epoxy composites, according to literature references (Tsai [49], Mil-HDBK-17 [50], Schwartz [51], Herakovich [52]), are in the following range: $120\ \text{GPa} \leq E_{11} \leq 200\ \text{GPa}$; $8\ \text{GPa} \leq E_{22} \leq 11\ \text{GPa}$; $3.5\ \text{GPa} \leq G_{12} \leq 8.5\ \text{GPa}$; $0.28 \leq \nu_{12} \leq 0.34$. This range is used as a basis to develop the present analytical study.

An expression for the reciprocal of the tangent of angle ϕ ($\cot \phi$) can be derived using equations (1) and (2); multiplying both the numerator and denominator of this expression by E_{11} leads to the following equation:

$$\cot\phi = -\frac{\left(2+2\nu_{12}-\frac{E_{11}}{G_{12}}\right)\sin\theta\cos^3\theta+\left(-2\nu_{12}-\frac{2E_{11}}{E_{22}}+\frac{E_{11}}{G_{12}}\right)\sin^3\theta\cos\theta}{\cos^4\theta+\left(-2\nu_{12}+\frac{E_{11}}{G_{12}}\right)\sin^2\theta\cos^2\theta+\frac{E_{11}}{E_{22}}\sin^4\theta}. \quad (3)$$

Let us define a variable μ as the quotient G_{12}/E_{11} to simplify the notation. From equation (3), we can derive an explicit formulation for the tab angle ϕ:

$$\phi = \arctan\left[\frac{\frac{1}{\tan^2\theta}-\left(2\nu_{12}-\frac{1}{\mu}\right)+\frac{E_{11}}{E_{22}}\tan^2\theta}{-\left(2+2\nu_{12}-\frac{1}{\mu}\right)\frac{1}{\tan\theta}+\left(\frac{2E_{11}}{E_{22}}+2\nu_{12}-\frac{1}{\mu}\right)\tan\theta}\right]. \quad (4)$$

As can be observed in equation (4), the parameters that ϕ depends on are the quotient $\mu = G_{12}/E_{11}$, the fibre orientation angle θ, the Poisson's ratio ν_{12}, and the quotient E_{11}/E_{22}. In figure 2, the variation in tab angle ϕ as a function of μ is represented for three fibre orientation angles (10º, 30º, 45º). For this graphical representation, the average values were used for both parameters ν_{12} (0.31) and quotient E_{11}/E_{22} (18) in the range of material properties considered.

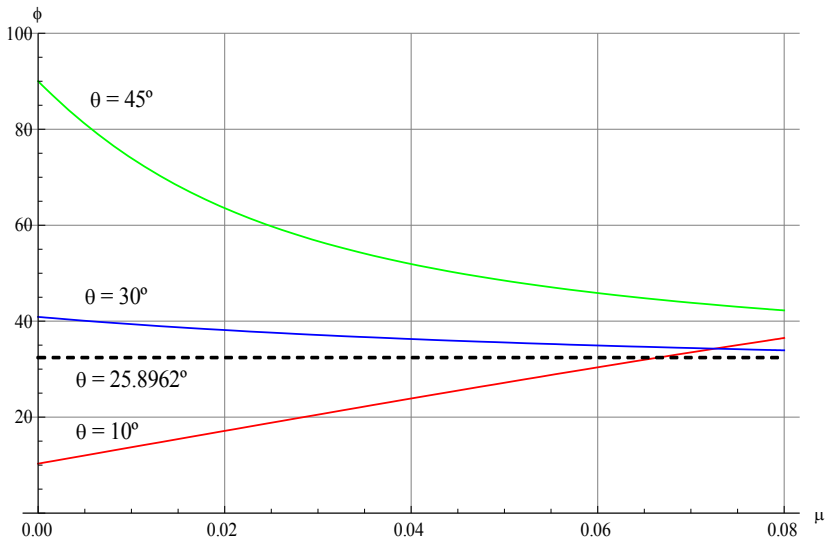

Figure 2. Variation in tab angle ϕ with μ for different fibre orientation angles θ (10º, 30º, 45º).

As can be observed in figure 2, the evolution of the graphs is linear for fibre orientation angles less than 30º, and it is nonlinear for angles greater than 30º. In view of the evolution of ϕ for fibre orientation angles less than 30º (which has an almost linear evolution), it can be deduced that an intermediate angle near 30º having a constant evolution of ϕ should exist. This intermediate angle is θ_ϕ = 25.8962º, in which ϕ = 32.4242º over the entire range of μ considered, i.e., for this orientation, the tab angle becomes nonsensitive to the variation in μ. Likewise, the variation in the tab angle ϕ with the Poisson's ratio ν_{12} in the range of properties considered (0.28, 0.34) can be evaluated; this shows that the Poisson's ratio has a negligible effect on the tab angle ϕ, as seen in figure 3.

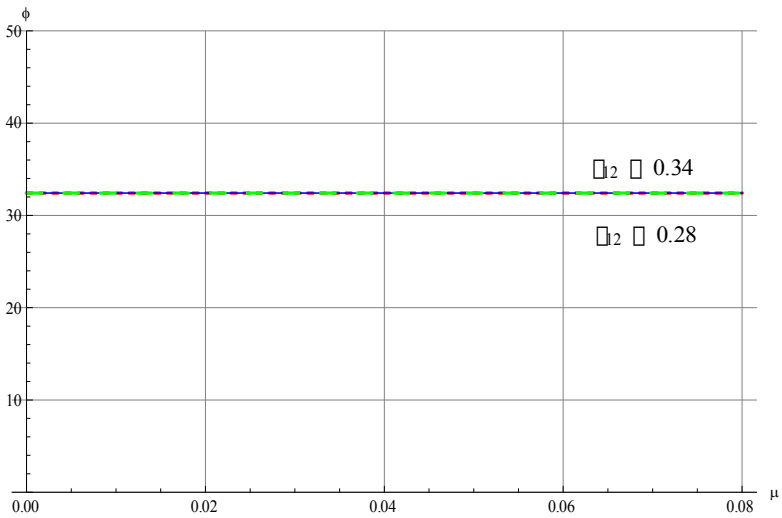

Figure 3. Variation in ϕ versus μ for θ = 25.8962º and for the extreme values of ν_{12} (0.28, 0.31).

The variation in quotient E_{11}/E_{22} produces a variation in ϕ, which affects the fibre orientation angle θ_ϕ defined previously. Table 1 shows the values of these orientations θ_ϕ for the central values and the extreme values of quotient E_{11}/E_{22} in the range of properties considered. The tab angles ϕ that correspond to these orientations are also presented in table 1.

Table 1. Fibre orientation angles θ_ϕ for which the evolution of ϕ is constant with μ.

E_{11}/E_{22}	θ_ϕ (º)	ϕ (º)
10.9	28.8214	38.2797
18	25.8962	32.4242
25	24.0948	29.2059

As seen from the values in table 1, fibre orientations θ_ϕ in the range of 24.1–28.8º led to minimal variation in the tab angle ϕ. To estimate the error of ϕ that we could commit by choosing a specific orientation θ, we have used an orientation $\theta = 26º$, which is approximately in the centre of the optimal interval. Figure 4 shows the evolution of the tab angle ϕ that corresponds to an orientation $\theta = 26º$ for the extreme and central values of the quotient E_{11}/E_{22}. As can be observed, the greatest angular deviations occur at the highest μ values. Thus, for $E_{11}/E_{22} = 10.9$, a maximum negative angular deviation of -3.80° is obtained, and for $E_{11}/E_{22} = 25$, a maximum positive angular deviation of +2.75° is obtained. These would be the maximum angular errors in the case of choosing $\phi = 32.5°$, which is the value associated with $\theta = 26°$ for the central value of the quotient $E_{11}/E_{22} = 18$.

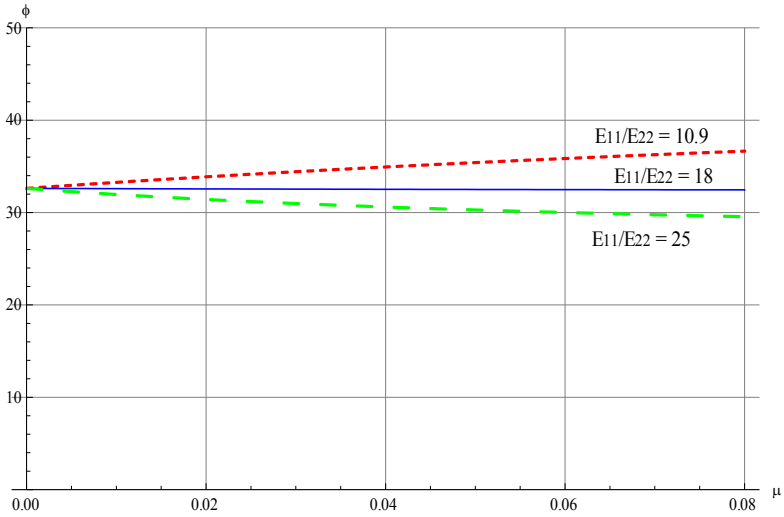

Figure 4. Variation of ϕ versus μ for θ = 26º and for different values of E_{11}/E_{22} (10.9, 18, 25).

After evaluating the possible maximum angular deviations of ϕ that could appear for a fibre orientation θ = 26°, it would be necessary to analyse if these deviations could be considered acceptable, i.e., the stress concentration generated by the angular deviation would not cause specimen failure. Pierron et al. [47], based on numerical studies, estimated that this error was ±3º for an orientation θ = 10º; however, the permissible error for different orientations is still unknown. For this purpose, it is necessary to analyse how the stress concentration at the corners of the specimen varies when there is a deviation in the angle of the tabs. A FEM 2D model of the problem has been made using the program ANSYS [53]; the model consists of 40000 SHELL63-type elements and 40501 nodes. The mesh, as seen in figure 5, has been conveniently refined in the area close to the specimen ends to better analyse the effect of the stress concentration in this area. To take into consideration how the stress concentration varies, a point (highlighted with a red circle in figure 5(B)) sufficiently close to the corner (0.2 mm) has been chosen as a preliminary indicator for comparison. The discretisation has been

verified by comparing the results for a mesh with an element size that has been reduced by half; the obtained results were equivalent at the considered point.

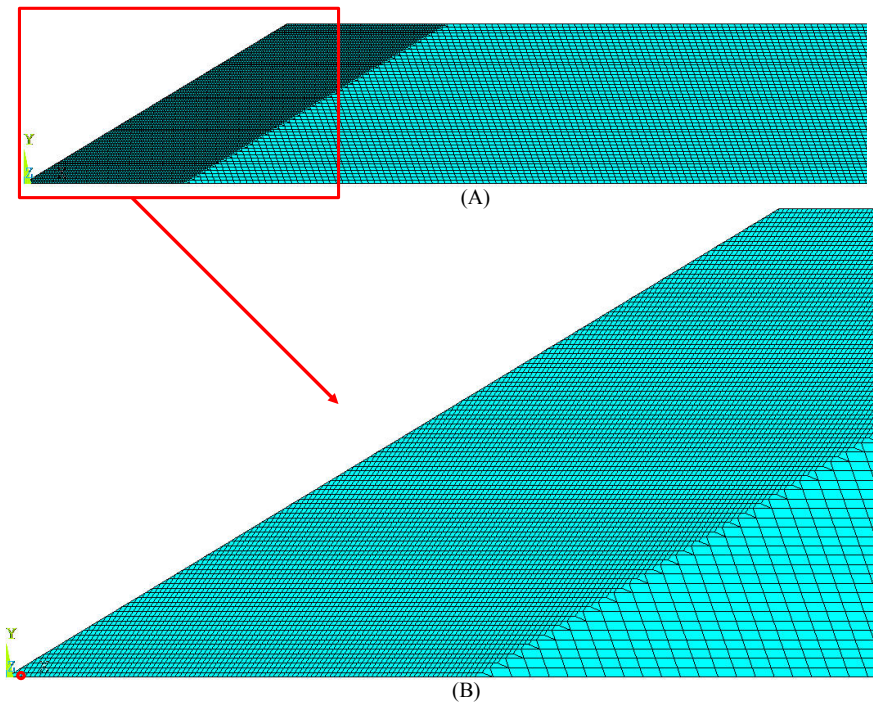

Figure 5. View of the mesh: (A) general view; (B) detailed view of the corner.

For graphite-epoxy composites, the following average values for each property (i.e., the average value of the entire range of considered values) were used for the FEM: E_{11} = 160 GPa; E_{22} = 9.5 GPa; G_{12} = 6 GPa; and ν_{12} = 0.31. Different orientations of the fibres have been considered, including θ = 5º, 10º, 15º, 20º and 26º. Figures 6(a), 6(b) and 6(c) show how the concentrations of stress components (σ_{11}, σ_{22}, σ_{12}) vary with the deviation in the tab angle $\Delta\phi$ at the selected point. Only positive deviations have been represented since they were the most unfavourable results. These concentrations have been evaluated as the quotient between the value of a particular stress component at the specified point and the value of the same stress component in the ideal configuration (identified by id in the figures) for the same load level. For all the orientation angles

considered, we observed that the stress concentrations increase with the angular deviation Δϕ. For a particular deviation, the stress concentrations generally increase with the orientation angle of the fibres.

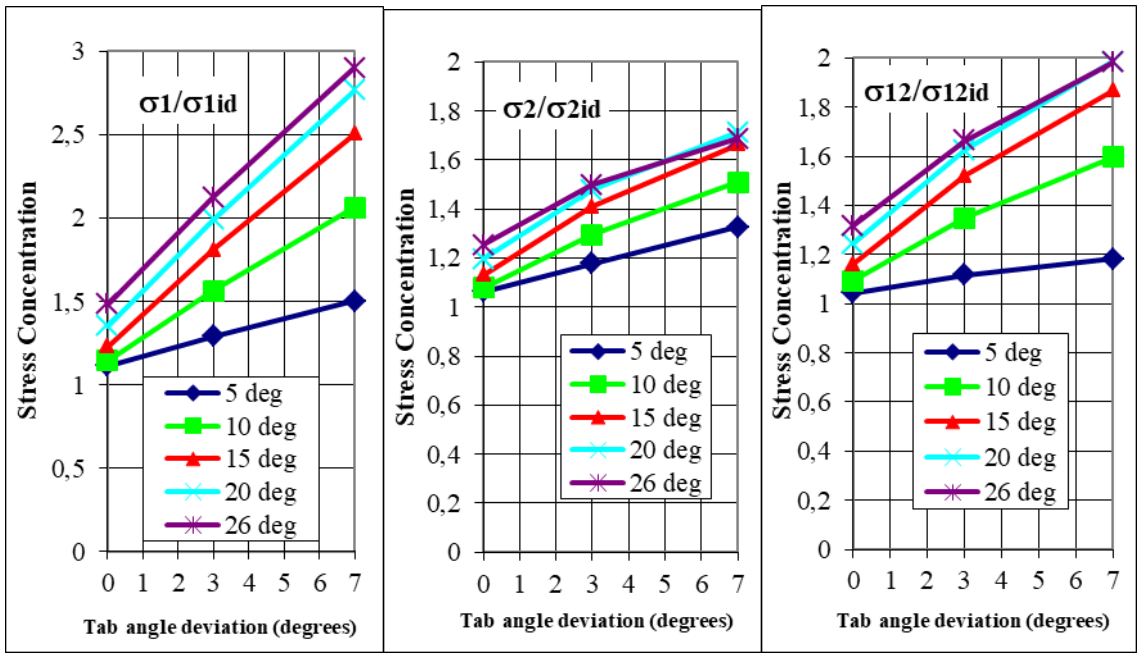

(a) (b) (c)

Figure 6. Variation in the stress concentration of: (a) σ_{11}, (b) σ_{22} and (c) σ_{12} with the angular deviation of the tabs Δϕ.

To take into account the contribution of these stress components to the failure of the specimen, it is necessary to use a failure criterion. In this study, we have used the theories of Tsai-Wu [54] and Puck [55], whose equations ((8) and (6), respectively) will be detailed in section 5. In each case, for an orientation θ and a deviation Δϕ, the stress state has been forced to take the values that would indicate failure in the ideal configuration (i.e., the failure criterion equations are set equal to unity). Then, the value of each failure criterion equation at the selected point (near the corner) has been represented in the following figures.

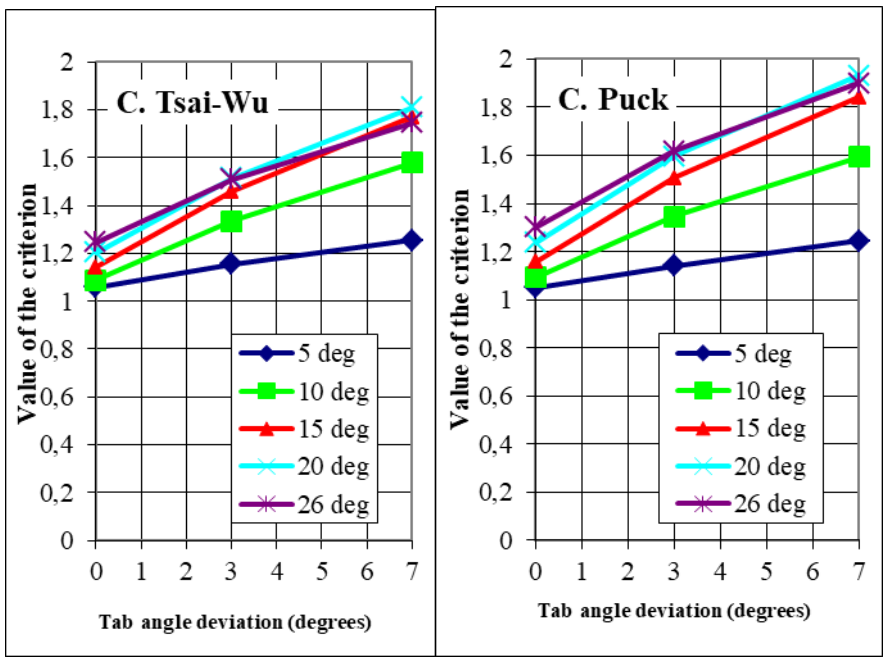

(a) (b)

Figure 7. Variation in the value of the criteria with the angular deviation of the tabs $\Delta\phi$: (a) Tsai-Wu C., (b) Puck C.

The variation in the value of the Tsai-Wu and Puck failure criteria with the deviation in tab angle $\Delta\phi$ is shown in figure 7, the results obtained with both theories being very similar. As with the stress components, it is observed that the value of the criteria increases with the angular deviation of tabs, and for each deviation $\Delta\phi$, the value of the criterion generally increases with the orientation of the fibres θ.

If we assume that the maximum acceptable level of the criterion is reached for an orientation $\theta = 10^{o}$ and a deviation $\Delta\phi = +3^{o}$ (as declared admissible by Pierron et al. [47]), this value of the criterion corresponds to approximately 1.34, as seen in figure 7. This assumption would imply that the allowable deviations would be less than +3° at orientations greater than 10º. Thus, for the cases where θ = 15°, 20°, and 26°, the failure criterion value would be 1.34 for deviations $\Delta\phi$ around +1.7°, +1.1° and +0.8°,

respectively. The allowable deviations would increase only in the case of fibre orientations less than 10°. Thus, for $\theta = 5°$, the acceptable level of the criterion would be reached with a deviation $\Delta\phi$ of approximately +9º. Therefore, for fibre orientations greater than 10º, the amount of potential angular deviation decreases, but the maximum acceptable deviations drastically reduce. In contrast, for fibre orientations of 10° and lower, the potential angular deviation may be greater, but the maximum acceptable deviation is also greater. Table 2 shows the potential deviations and the estimated acceptable deviations for the different orientations analysed. It should be mentioned that negative acceptable deviations have been recorded alongside the positive deviations, but in this particular case, we can say that these values would represent a minimum of the acceptable deviations. As previously mentioned, negative deviations with respect to the angle of the tabs are less unfavourable than the positive deviations, and therefore, they lead to lower stress concentrations.

Table 2. Potential deviations in tab angle ϕ and acceptable deviations $\Delta\phi$.

θ (º)	Theoretical ϕ (º)	Potential deviation in ϕ (º)	Acceptable deviation $\Delta\phi$ (º)
5	29.6	±15.4	±9
10	23.1	±9.1	±3
15	24.2	±5.9	±1.7
20	27.5	±4	±1.1
26	32.5	+2.8 -3.8	±0.8

It should be noted that the consequences obtained are based on the numerical results of the model studied, and, as previously mentioned, the stress state at the corner is

singular. A singular stress state analysis is carried out in the next section to give more representativeness to the previously obtained results.

4. Study of the singular stress state at the corners of the specimen.

Experimental evidence shows that premature undesirable failures near the tabs of the specimen typically occur in configurations with oblique tabs, as seen in figure 8.

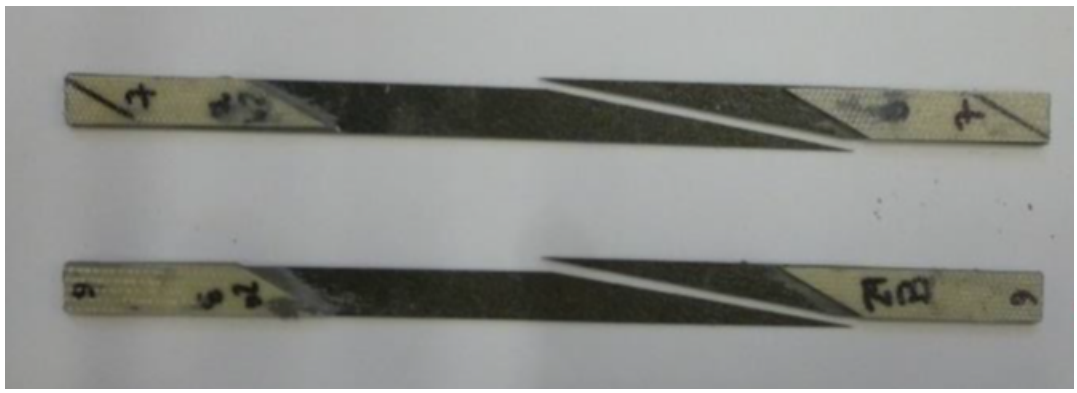

Figure 8. Premature failures in off-axis samples with oblique tabs.

To analyse the role of the singular stress states induced by the presence of a corner at the end-tabs of the specimen, a specific study of the stress singularities has been carried out.

Considering a planar model of the specimen, the orders of stress singularities, δ in $\sigma_{\alpha\beta}(r,\theta) \approx \sum_k K_k r^{\delta_k} f_{\alpha\beta}^{(k)}(\theta)$ (with a polar coordinate system centred at the corner tip, and where K and $f_{\alpha\beta}(\theta)$ are the generalized stress intensity factor and the characteristic angular function, respectively [56]), have been evaluated for different combinations of the fibre and tab angles, θ and ϕ. The calculations have been carried out using the semi-analytical procedure developed by Barroso et al. [56]. The procedure is fully analytical

with the exception of a final numerical search for the roots (the orders of stress singularities) of the characteristic equation; the accuracy of this procedure is extremely good (up to 13 digits), which has been demonstrated in a previous work by Mantic et al. [57].

The tool used for the stress singularities at multimaterial corners allows any number of elastic wedges converging at the same corner and any type of linear elastic constitutive law, any perfect adhesion or sliding friction contact between material wedges, and any general homogeneous boundary conditions imposed along the external faces (in case of open corners) or closed corners (all material wedges being connected), to be taken into consideration [56,57]. The tool also allows the presence of the so-called mathematically degenerate materials in the framework of the Stroh formalism of anisotropic elasticity in complex variable, which is the base of the code. With such characteristics, the present tool is, to the best authors' knowledge, one of the few available codes to determine the order of stress singularities with these types of materials and boundary conditions.

The procedure is able to evaluate complex-valued orders of stress singularities, which typically appear in interface cracks in bimaterial configurations. This fact implies that the generalized stress intensity factors are also complex number, which is not the case for the problem under analysis. The program also incorporates the argument principle, which is an excellent tool for identifying the number of roots of a holomorphic function in a particular region of the complex plane, which allows all orders of stress singularities to be perfectly identified and evaluated. As a final consideration of the program characteristics, it can evaluate a singular stress field with multiple terms, all of them being singular. In the problem under analysis, only one singular term appears, allowing a straightforward interpretation of the results.

In the particular problem under analysis, where the free edge of the sample is used as the horizontal reference direction, the corner configuration consists of a single orthotropic material wedge that is free along the lateral side of the specimen and clamped along the side of the specimen inclined an angle ϕ; the fibre orientation θ is measured counterclockwise from the free edge.

A detailed view of the left end of an off-axis specimen is shown in Figure 9, where the two corner configurations that generate stress singularities are identified as corner A and corner B. Due to the properties in the homogeneous 2D model associated with the internal structure (orientation of the fibres) at both corners, only corner A will be considered hereafter. A failure that initiates at corner A via a combination of shear and circumferential (normal) stresses can progress throughout the matrix, parallel to the fibre direction, all along the specimen, thereby generating a catastrophic failure. However, a failure that initiates at corner B via a combination of shear and circumferential (normal) stresses can only progress by means of fibre failure, which is, of course, less likely to occur than the matrix failure at corner A.

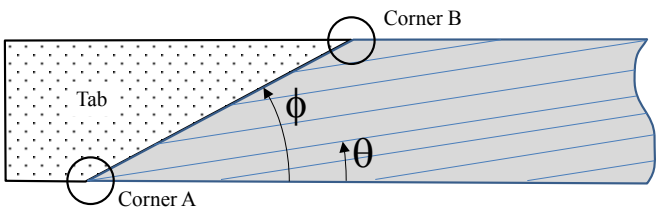

Figure 9. Detailed view of the corners at the specimen end, which generate stress singularities.

Figure 10 shows the orders of stress singularities for five different fibre angles (θ = 5º, 10º, 15º, 20º, 26º) and various tab angles from the straight configuration (ϕ = 90º) to that (15º) giving a negative order of stress singularity (i.e.: no unbounded stresses).

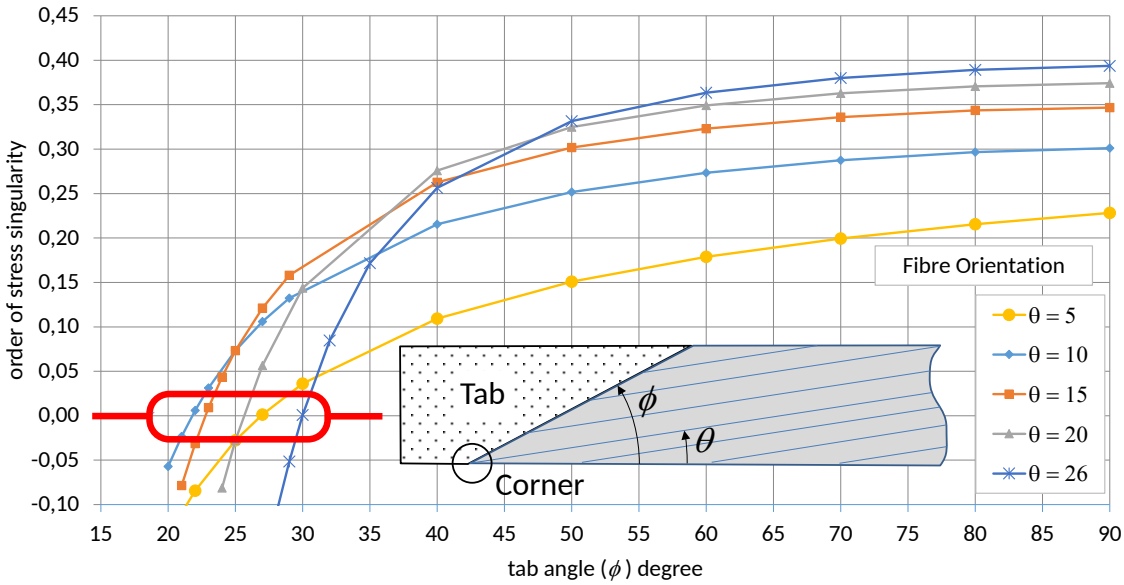

Figure 10. Orders of stress singularity δ at corner A for various combinations of fibre angles (θ = 5º, 10º, 15º, 20º, 26º) and tab angles (20º<ϕ <90º).

It can be observed in Figure 10 that the behaviour for all five fibre angles is similar in the sense that the higher the tab angle is, the higher the order of stress singularity. Additionally, it can be observed that the order of stress singularity associated with the theoretical ϕ (see Table 2) for each orientation θ increases with the angle of the fibres. Consequently, fibre orientation angles of 5º and 10º would be more appropriate in this sense, as they result in smaller orders of stress singularity at corner A.

Assuming the maximum acceptable level in the order of stress singularity to be the one that is reached at a fibre orientation θ = 10º and a tab angle deviation Δϕ = +3º, as has been done previously in the stress results from the numerical analysis, we can

determine, based on a nominal singular stress state, the acceptable deviations $\Delta\phi$ for different fibre orientations. Table 3 shows the estimated values of the acceptable deviations for the different orientations θ considered.

Table 3. Estimated values of the acceptable .

θ (º)	Theoretical ϕ (º)	Acceptable deviation $\Delta\phi$ (º)
5	29.6	+8
10	23.1	+3
15	24.2	+1.6
20	27.5	+0.75
26	32.5	+0

As can be observed, the values of the allowable deviations estimated on the basis of the analytical study of the order of stress singularity (Table 3) are very similar to those obtained on the basis of numerical models (Table 2), i.e., both showed the same trend. It should be noted that the results of the study of stress singularity are more restrictive, as they estimate lower values of deviations. In the particular case where the fibre orientation angle θ is 26°, no positive deviation would be allowable according to the study of stress singularity.

Another important consequence that can be observed in figure 10 is that negative $\Delta\phi$ deviations contribute to a decrease in the order of stress singularity at the corner. For each orientation θ, there will be a certain negative deviation that eliminates the stress

singularity ($\delta = 0$). These points have been highlighted by a red rectangle in figure 10. From the fibre orientations considered, $\theta = 10^{o}$ is the one in which the theoretical angle of the tabs ($\phi = 23.1^{o}$) is closest to the angle that produces $\delta = 0$ (21.8^{o}). For that reason, the 10^{o} orientation could be considered optimal in terms of the singularity of the nominal stress state at the corner (in the neighbourhood of the corner).

Another fact to be emphasised, which can be deduced from the results presented in figure 10, is that the stress singularity orders that correspond to the straight tab configuration ($\phi = 90°$) are greater than those of the oblique tab configuration for all the fibre orientations considered. Therefore, the configuration of oblique tabs would be more favourable than that of straight tabs in terms of the stress severity levels that appear in the corners.

5. Study of the optimal fibre orientation θ for the determination of shear strength.

As previously mentioned in the introduction section, the stress state in the off-axis test is not a pure shear stress field; therefore, these tests require the application of a failure criterion for the indirect determination of shear strength S. Chamis & Sinclair [15], using the Chamis criterion, identified that orienting the fibres at 10^{o} is suitable because the term associated with the shear stress σ_{12} is dominant in comparison to those terms associated with the normal stresses. Following this recommendation, the orientation $\theta = 10^{o}$ is the most used configuration in the off-axis test with regular tabs. In the recent work by Vargas & Mujika [42], we can find similar discussions that propose this particular fibre orientation above others. In particular, regarding the oblique tab configuration, the 10^{o} orientation has been one of the most frequently used [45, 47, 48, 58, 59]. Nevertheless, other orientations have also been used with the oblique tab configuration as for example in the original proposal by Sun & Chung [20] where a 20^{o}

orientation is used, or in the works by Xiao et al. [22] and Xavier et al. [60] where a 15º orientation is employed.

To determine which fibre orientation angle is best suited for shear strength determination under an oblique tabs configuration, it is necessary to analyse when the failure will take place, and under which stress state it will occur. For the failure determination, it is necessary to select a failure criterion; two of the proposals that have had the best results in the world wide failure exercise [61], Puck's criterion [55] and Tsai-Wu's criterion [62], were selected in the present work.

Regarding the stress state at the instant that failure occurs in the oblique tabs configuration, the one appearing in the central area of the specimen, which will be considered to be approximately equal to the one in the ideal off-axis configuration, will be assumed. This hypothesis is supported by the numerical results [20, 45] and experimental results [46, 47] of previous works in the literature. Thus, we can assume that the stress state under which the failure takes place can be approximated as follows:

$$\sigma_{11} = \sigma_x \cos^2\theta \quad ; \quad \sigma_{22} = \sigma_x \sin^2\theta \quad ; \quad \sigma_{12} = -\sigma_x \sin\theta\cos\theta\,, \tag{5}$$

where σ_x is the applied longitudinal stress.

With the stress state given by (5), the activated failure mode, according to Puck's criterion [55], would be the "inter-fibre failure mode A", whose equation is given by:

$$\sqrt{\left(\frac{\sigma_{12}}{S}\right)^2 + \left(1 - P_{\perp\parallel}^{(+)}\frac{Y_T}{S}\right)^2\left(\frac{\sigma_{22}}{Y_T}\right)^2} + P_{\perp\parallel}^{(+)}\frac{\sigma_{22}}{S} = 1 - \left(\frac{\sigma_{11}}{1.1X_T}\right)^6, \tag{6}$$

where $P_{\perp\parallel}^{(+)}$ is 0.35 for graphite composites, as recommended by the author. Through a convenient manipulation, equation (6) is transformed into:

$$\left(\frac{\sigma_{12}}{S}\right)^2+\left(1-2P_{\perp\parallel}^{(+)}\frac{Y_T}{S}\right)\left(\frac{\sigma_{22}}{Y_T}\right)^2+2P_{\perp\parallel}^{(+)}\frac{\sigma_{22}}{S}-\left[2P_{\perp\parallel}^{(+)}\frac{\sigma_{22}}{S}-2+\left(\frac{\sigma_{11}}{1.1X_T}\right)^6\right]\left(\frac{\sigma_{11}}{1.1X_T}\right)^6=1 \quad (7)$$

where the term associated with σ_{12} can be isolated from the rest, which makes it easier to evaluate its contribution to the criterion apart from the contributions of the other stress terms. For that aim, all possible values of angular orientations have been covered, from 0º to 90º, at intervals of 1º. Moreover, for each angle, the value of σ_x that gives rise to the failure was obtained by means of solving equation (7) for the stress term showed in (5). Using these values of σ_x, the difference between the term associated with σ_{12} and the sum of the rest of the terms can be evaluated. When this difference is positive, it means that the term associated with σ_{12} is dominant. The optimum orientation corresponds to the angle for which this difference is maximum.

Taking various sources for the mechanical properties of graphite-epoxy composites [49-52], the ratio Y_T/S typically varies between 0.4227 and 0.7282, and the tensile strength in the fibre direction X_T varies between 1200 MPa and 2900 MPa. After making the aforementioned evaluations and calculations for the distinct combinations of the mechanical properties of the materials (Y_T, X_T, S) for the previously mentioned range of values, the intervals and optimum orientations are obtained and summarized in Table 4.

Table 4. Allowable angular intervals and optimum orientations according to Puck's criterion.

Y_T/S	X_T = 1200 MPa		X_T = 1800 MPa		X_T = 2900 MPa	
0.4227	(4º, 21º)	8º	(3º, 21º)	6º	(2º, 21º)	4º
0.6667	(4º, 30º)	8º	(3º, 30º)	6º	(2º, 30º)	4º
0.7282	(3º, 32º)	7º	(2º, 32º)	5º	(2º, 32º)	3º

With the results of Table 4, the interval of orientations in which it can be assumed that the shear stress term is dominant, i.e., the intersection of all intervals, would lie between 4º and 21º. The maximum values of the computed differences lie between 3º and 8º. Discarding the angle of 3º, which is outside the allowable interval, it can be stated that the optimum interval lies between 4º and 8º. Thus, according to Puck's criterion, the previous intervals ((4º, 21º) and (4º, 8º)) would be the allowable and optimum orientation intervals, respectively, for the determination of shear strength by means of off-axis tension tests.

With reference to Tsai-Wu's criterion [54], it is given by the following equation:

$$\left(\frac{\sigma_{12}}{S}\right)^2+\frac{\sigma_{11}^2}{X_T X_C}+\frac{\sigma_{22}^2}{Y_T Y_C}+\left(\frac{1}{X_T}-\frac{1}{X_C}\right)\sigma_{11}+\left(\frac{1}{Y_T}-\frac{1}{Y_C}\right)\sigma_{22}-\sqrt{\frac{1}{X_T X_C Y_T Y_C}}\sigma_{11}\sigma_{22}=1 \quad (8)$$

.

Following the same procedure previously outlined for Puck's criterion, and assuming the same variation ranges of the mechanical properties (X_T, X_C, Y_T, Y_C, S), the orientation interval for which the shear stress term is dominant can be determined. In this case, besides the variation ranges of X_T (1200 MPa, 2900 MPa) and the ratio Y_T/S (0.4227, 0.7282) previously considered, it is necessary to take into account the variation in X_C/X_T (0.58, 0.89) and Y_C/Y_T (3.37, 5.31). In Table 5, the allowable intervals and

optimum orientations obtained for different combinations of the mechanical properties are shown.

Table 5. Allowable angular intervals and optimum orientations according to the Tsai-Wu criterion.

Y_T/S	X_T (MPa)	$X_C/X_T = 0.58$ $Y_C/Y_T = 3.37$	$X_C/X_T = 0.58$ $Y_C/Y_T = 5.31$	$X_C/X_T = 0.89$ $Y_C/Y_T = 3.37$	$X_C/X_T = 0.89$ $Y_C/Y_T = 5.31$
0.4227	1200	(5º, 22º) 10º	(5º, 21º) 9º	(5º, 20º) 10º	(5º, 19º) 9º
	2900	(2º, 20º) 5º	(2º, 19º) 5º	(2º, 19º) 6º	(2º, 18º) 5º
0.7282	1200	(4º, 33º) 9º	(4º, 32º) 9º	(4º, 31º) 10º	(4º, 30º) 10º
	2900	(2º, 31º) 5º	(2º, 30º) 5º	(2º, 31º) 6º	(2º, 29º) 5º

The interval of allowable orientations will be the intersection of all obtained intervals for the different combinations of mechanical properties, which in this case is (5º, 18º). In each one of the evaluated cases, the optimum orientation inside the corresponding interval was determined, which showed that all these orientations occurred in the range of (5º, 10º).

With the results of the different failure criteria considered, an interval of allowable orientations, which is evaluated as the intersection of the intervals obtained for the different criteria, can be determined; this interval is (5º, 18º). For all orientations inside this interval, it can be stated that the shear stress term σ_{12} is dominant according to the two considered failure criteria. The range where the optimum orientations are located could be defined as the combination of the optimum intervals, which would correspond to the interval (4º, 10º), where the maximum of the differences are located for all failure

criteria. As done previously for Puck's criterion, the lowest part of the interval (4º) will be discarded, as it falls outside of the allowable interval; therefore, the optimum orientation interval is reduced to (5º, 10º).

6. Experimental study.

A graphite-epoxy composite denominated AS4/8552 and manufactured by HEXCEL Composites has been considered at the present work. The average values of material properties, obtained from the available manufacturer's data, are:

$$E_{11} = 135 \text{ GPa} , E_{22} = 8.75 \text{ GPa} , G_{12} = 4.75 \text{ GPa} , \nu_{12} = 0.3. \quad (9)$$

These values allow the tab angles for the different fibre orientation in the off-axis tests to be estimated. These values of the tab angle can present certain deviation due to the uncertainty in the values of material properties. To check how correct the estimated tab angles are, 0º and 90º tension tests have been carried out additionally. For this purpose, two unidirectional panels with fibre orientation at 0º and 90º have been manufactured to determine the elastic modulus E_{11} and E_{22}, and the allowable values X_T and Y_T for the material considered. The panel with fibre orientation 0º has been prepared by laying up 4 pre-preg layers with dimensions 220x150 mm^2 with a resultant thickness of 0.85 mm approximately. The panel with fibre orientation 90º has been prepared by laying up 6 pre-preg layers with dimensions 200x150 mm^2 with a resultant thickness of 1.18 mm approximately. Both panels have been cured in autoclave, and then woven fabric glass fibre tabs have been joined to the ends of the panels. Rectangular specimens have been obtained from the panels by cut-out. From the 0º panel, 9 specimens with dimensions 200x10 mm^2 have been obtained, presenting regular tabs with 40 mm length approximately, and a specimen ratio L/w > 10 (L = free length, w = width). From the 90º panel, 8 specimens with dimensions 200x15 mm^2 have been obtained, presenting regular tabs with 50 mm length approximately, and a specimen ratio L/w = 6.67.

The tensile tests have been carried out in an INSTRON 4483 universal testing machine, with a 150 KN load cell, and a 50 mm length extensometer. The room temperature for tests was 22ºC, the relative humidity was 50%, and the displacement velocity was 1 mm/min. As results of the 0º tension tests the average values for both the elastic modulus in fibre direction E_{11}, the tensile strength in fibre direction X_T and the failure strain in fibre direction $X_{\varepsilon T}$ have been obtained. These average values with their corresponding standard deviations (STD) are:

E_{11} = 125.159 GPa (STD: 2.615 GPa) ; X_T = 1746.458 MPa (STD: 36.079 MPa) ; $X_{\varepsilon T}$ = 1.394% (STD: 0.029 %).

As results of the 90º tension tests the average values for both the elastic modulus perpendicular to the fibre direction E_{22}, the tensile strength perpendicular to the fibre direction Y_T and the failure strain perpendicular to the fibre direction $Y_{\varepsilon T}$ have been obtained. These average values with their corresponding standard deviations are:

E_{22} = 8.112 GPa (STD: 0.232 GPa) ; Y_T = 53.666 MPa (STD: 4.875 MPa) ; $Y_{\varepsilon T}$ = 0.662 % (STD: 0.060 %).

Four rectangular panels with fibre orientation angles 5º, 10º, 15º and 20º have been manufactured by laying up 4 pre-preg layers, the dimensions of these panels are respectively: 215x123 mm^2, 207x115 mm^2, 208x97 mm^2, and 199x88 mm^2. From the 5º panel, 8 specimens with dimensions 202x10 mm^2 have been obtained; 7 specimens from the 10º panel with dimensions 200x10 mm^2; 6 specimens from the 15º panel with dimensions 205x10 mm^2; and 6 specimens from the 20º panel with dimensions 198x10 mm^2.

On the basis of the average values of material properties (9), and using equation (4), the tab angle ϕ for every different fibre orientation θ can be estimated. These angles are shown in table 6.

Table 6.- Estimated and practical tab angles for the different fibre orientation.

θ (º)	5	10	15	20
ϕ (º)	28.23	22.36	23.8	27.44
ϕ_p (º)	28	22	24	27

Due to the difficulty in precisely cut these estimated angles, practical tab angles ϕ_p have been selected, as shown in table 6. Using these practical angles ϕ_p woven fabric glass fibre tabs have been cut with a length of 40 mm approximately, 10 mm width and trapezoidal shape. These oblique tabs have been bonded to specimens by means of SAFRAN adhesive.

The off-axis tensile tests have been carried out in an INSTRON 4483 universal testing machine, with a 150 KN load cell, and a 50 mm length extensometer. The room temperature for the tests, the relative humidity and the displacement velocity have been respectively, 22ºC, 50% and 1 mm/min. Mechanical grips have been used in the tests, and all the surface of the tab was griped to try to reproduce the displacement boundary condition at the end of specimen. Experimental curves of longitudinal stress σ_x versus longitudinal strain ε_x are shown in figure 11. Due to the uniformity of stress field at the central zone of specimen, it must be mentioned that measured values (which are average values) of both stress and strain are representatives of the values at the points in this central zone.

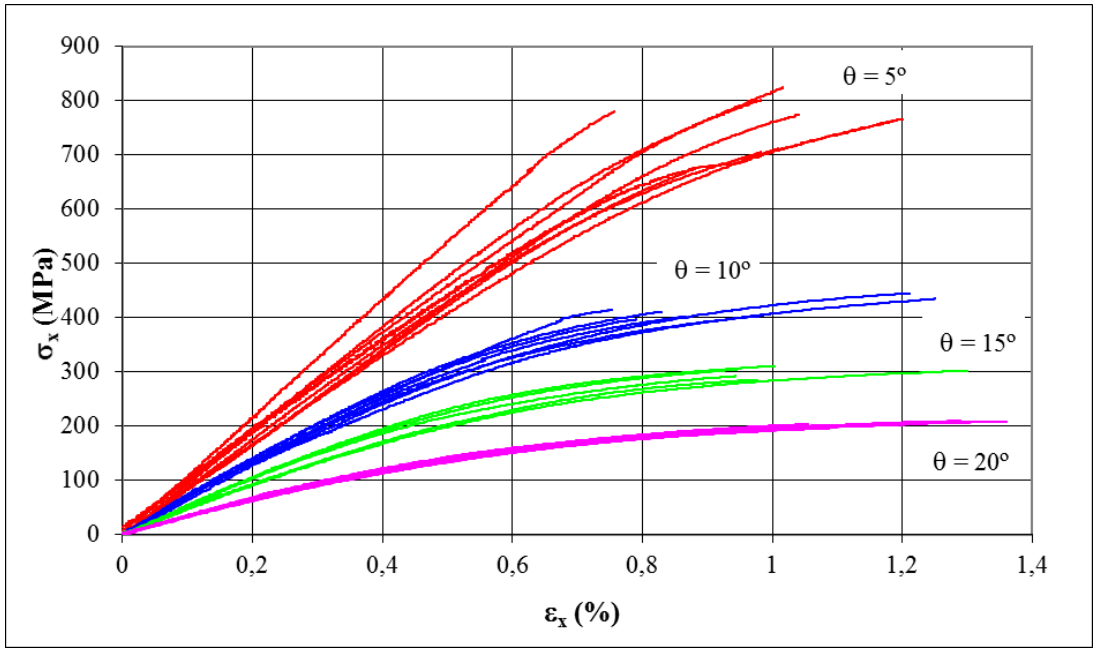

Figure 11.- Stress-strain curves (σ_x vs. ε_x) for the different fibre orientations considered.

As is shown in figure 11, the scattering in the behaviour of specimens decreases with the increase in the fibre orientation angle θ, it being maximum for 5º and almost negligible for 20º. The average values of the tensile strength σ_{xu} and the failure strain ε_{xu} with their corresponding standard deviations are shown in table 7. The elastic modulus E_x (slope at the beginning of the curves) and the secant value of the modulus E_{xsec} ($E_{xsec} = \sigma_{xu} / \varepsilon_{xu}$) are also shown in table 7.

Table 7.- Failure stress and strain, and elastic modulus.

θ (º)	σ_{xu} (MPa)	STD (MPa)	ε_{xu} (%)	STD (%)	E_x (GPa)	E_{xsec} (GPa)
5	753.539	53.792	0.976	0.119	92.574	76.043
10	414.945	17.850	0.989	0.198	70.928	43.053
15	296.842	10.063	1.034	0.150	50.204	29.284
20	200.602	12.585	1.140	0.231	33.889	18.122

The failures observed in specimens with fibre directions 5º, 10º, 15º and 20º are shown in figures 12, 13, 14 and 15 respectively. As can be seen in figure 12, all specimens with fibre orientation angle θ =5º present failures near the corners. As can be seen in figure 13, the specimens with fibre orientation 10º fail mainly at the central zone (5 failures at central zone, 1 failure at lateral zone, 1 failure at the corner). As can be seen in figure 14, the majority of specimens with fibre orientation 15º fail at the lateral zone (5 failures at lateral zone, 1 failure at central zone). Finally, as can be seen in figure 15, the specimens with fibre orientation 20º fail mainly at the lateral zone (5 failures at lateral zone, 1 failure at central zone).

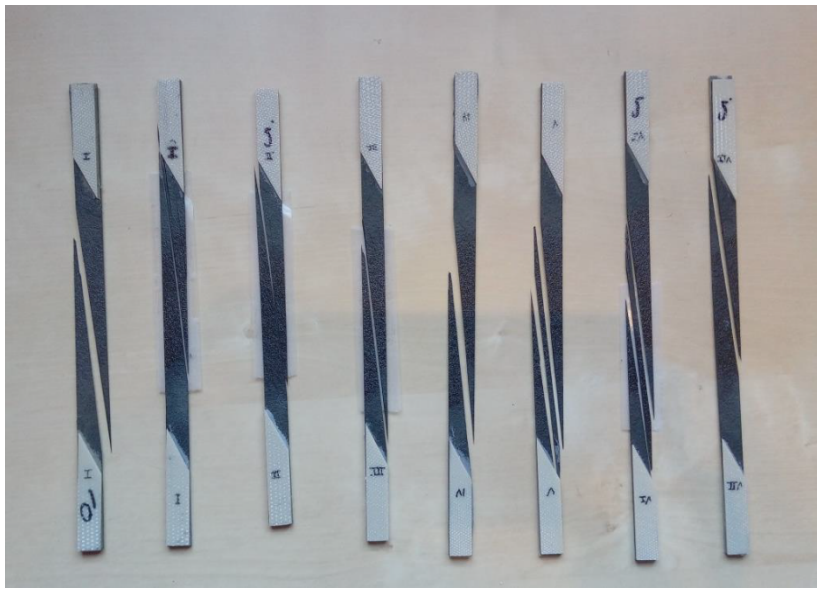

Figure 12.- View of the failure specimens for fibre orientation angle 5º.

Figure 13.- View of the failure specimens for fibre orientation angle 10º.

Figure 14.- View of the failure specimens for fibre orientation angle 15º.

Figure 15.- View of the failure specimens for fibre orientation angle 20º.

7. Analysis of experimental results and discussion.

The shear properties of the material considered (modulus G_{12} and strength S) are the values that are wanted to be obtained from the direct results of tests (longitudinal modulus E_x and failure stress σ_{xu}). In what concerns to the shear modulus G_{12}, this property can be evaluated by means of the following expression:

$$\frac{1}{E_x} = \frac{\cos^4\theta}{E_{11}} + \left(-\frac{2\nu_{12}}{E_{11}} + \frac{1}{G_{12}} \right) \sin^2\theta \cos^2\theta + \frac{\sin^4\theta}{E_{22}} \qquad (10)$$

Substituting the E_x values (see table 7) in equation (10) and the experimental values of both E_{11} and E_{22} (E_{11} = 125.159 GPa, E_{22} = 8.112 GPa), with the Poisson's ratio of the

material (ν_{12} = 0.3), the shear modulus G_{12} for every fibre orientation θ can be evaluated. The G_{12} values for the different orientations θ are shown in table 8. The values of the secant shear modulus G_{12sec}, which can be obtained from equation (10) using the secant longitudinal modulus E_{xsec} (see table 7), are shown also in table 8.

Table 8.- Shear modulus G_{12} and G_{12sec}.

θ (º)	G_{12} (GPa)	G_{12sec} (GPa)
5	2.545	1.419
10	4.423	1.858
15	4.917	2.320
20	4.677	2.163

As can be observed from the values in table 8, a high difference exists between the value of the shear modulus G_{12} (slope at the beginning) and the value of the secant shear modulus G_{12sec}. The meaning of this difference is obviously the non-linear character of the shear behaviour. Therefore, to characterise the material behaviour the knowledge of shear curve (σ_{12} vs. γ_{12}) is needed. For this purpose, the shear stress component σ_{12} can be evaluated from the longitudinal stress σ_x using the equation (5) corresponding to the stress field of the ideal off-axis tension test configuration (figure 1(a)). The shear strain γ_{12}, according to the material constitutive law in orthotropic axes, can be expressed as the quotient σ_{12}/G_{12}. In this way, using equation (5) and the constitutive law in geometric axes of specimen ($\sigma_x = E_x \cdot \varepsilon_x$), the following expression is obtained:

$$\gamma_{12} = -\frac{\sigma_x \sin\theta\cos\theta}{G_{12}} = -\frac{E_x \varepsilon_x}{\sin\theta\cos\theta} \cdot \frac{\sin^2\theta\cos^2\theta}{G_{12}} \qquad (11)$$

Using equation (10), the above expression becomes:

$$\gamma_{12} = -\frac{E_x \varepsilon_x}{\sin\theta\cos\theta} \cdot \left(\frac{1}{E_x} - \frac{\cos^4\theta}{E_{11}} + \frac{2\nu_{12}}{E_{11}} \sin^2\theta\cos^2\theta - \frac{\sin^4\theta}{E_{22}} \right) \tag{12}$$

Manipulating adequately equation (12) we can obtain:

$$\gamma_{12} = -\frac{\varepsilon_x}{\sin\theta\cos\theta} + \sigma_x \cdot \left(\frac{\cos^3\theta}{\sin\theta E_{11}} - \frac{2\nu_{12}}{E_{11}} \sin\theta\cos\theta + \frac{\sin^3\theta}{\cos\theta E_{22}} \right) \tag{13}$$

As can be observed in equation (13), the shear strain γ_{12} is expressed as a function of both the measured values in the tests (σ_x, ε_x) and constant values that depend on the fibre orientation angle θ and the material properties (E_{11}, E_{22}, ν_{12}). A direct measurement of γ_{12} can be obtained by instrumentation of specimens with 3 strain gages. This procedure is independent of material properties but is more expensive. Thus, using equations (5) and (13) the curves σ_{12} vs. γ_{12} for the different orientations considered can be evaluated. These curves are represented in figure 16.

As can be seen in figure 16, the scattering in the shear behaviour decreases with the increase in the fibre orientation angle θ, it being higher for 5º and smaller for 20º. Theoretically it might be expected that all fibre orientations presented the same shear behaviour, but it can be observed that the curves for θ = 5º shows a more flexible behaviour than the other orientations, leading to G_{12} values smaller than for the other cases. A possible explanation of this fact can be that for small fibre orientation angles, as θ = 5º, the material behaviour is dominated by the fibre. For that reason, variables

associated with the matrix, as the shear strain γ_{12}, can present significant errors. Therefore, the fibre orientation angle $\theta = 5^{o}$ can not be considered adequate to evaluate the shear modulus by means of the off-axis tension test with oblique end-tabs.

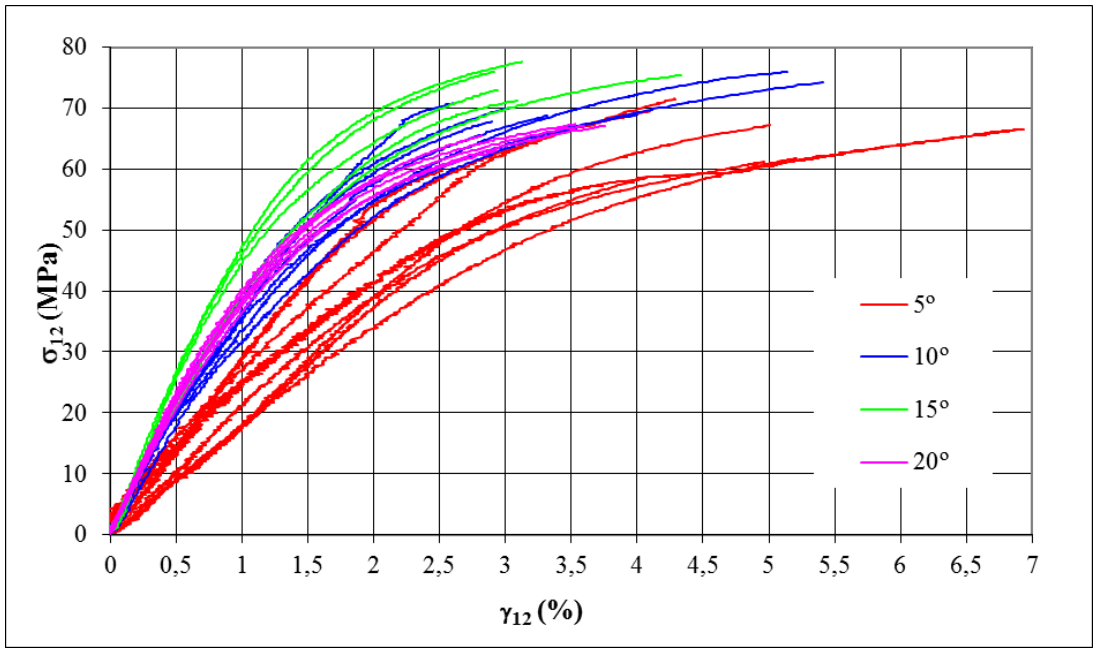

Figure 16.- Curves σ_{12} vs. γ_{12} for different orientations.

With reference to the other orientations (10º, 15º, 20º), the differences noticed in shear behaviour are small, it being observed that 10º and 20º orientation angles show a similar behaviour, while the specimens for $\theta = 15^{o}$ present a slightly stiffer behaviour than the others.

In what concerns to the evaluation of shear strength S, taking into account that the stress field in the specimens is a full stress state, with three components (σ_1, σ_2, σ_{12}), the use of a failure criterion is needed to evaluate S in an inverse manner. For this purpose, in this work, the theories of Puck [55] and Tsai-Wu [54] will be used again.

Theoretically, in the off-axis tension test with oblique end-tabs it can be supposed that the failure appears in the central zone of specimen, under a uniform stress field very approximated to that of the ideal test configuration, which can be expressed by equation (5). Therefore, the stress component values (σ_{1u}, σ_{2u}, σ_{12u}) in the central zone of specimen at the failure instant can be calculated substituting the experimental values of σ_{xu} (see table 7) in expression (5). These stresses values for the different orientations are shown in table 9.

Table 9.- Stress components in the regularized zone at failure.

θ (º)	σ_{1u} (MPa)	σ_{2u} (MPa)	σ_{12u} (MPa)
5	747.815	5.724	65.425
10	402.433	12.512	70.960
15	276.957	19.885	74.210
20	177.136	23.466	64.472

As can be observed from the values in table 9, the stresses in the central zone of specimens at the failure instant are different for the different orientations, and then, every orientation must be analysed separately. Previously, to address the analysis of the strength behaviour for every orientation, the angle of the tabs employed ϕ_p (estimated on the basis of the average values of material properties (9)) must be checked to verify that agrees with the theoretical values associated with the material properties (experimental values: E_{11} = 125.159 GPa, E_{22} = 8.112 GPa, G_{12} = 4.6 GPa, ν_{12} = 0.3). These theoretical values can be evaluated substituting the material properties in expression (4), these values together with the values of ϕ_p (for comparison purposes) are shown in table 10.

Table 10.- Theoretical and practical tab angles for the different fibre orientation.

θ (º)	5	10	15	20
ϕ (º)	27.74	22.10	23.63	27.35
ϕ_p (º)	28	22	24	27

As can be seen from the values in table 10, the tab angles ϕ_p used in specimens present deviations lesser than 0.5º, and therefore, they can be acceptable. This fact shows that the tab angles can be precisely evaluated on the basis of an estimation of material properties.

As is shown in figure 12, the majority of specimens for $\theta = 5º$ fails near the corner, where there is a singularity in the stress state (as can be seen in section 4). For that reason, this orientation is not suitable for the evaluation of shear strength S.

For $\theta = 10º$, as can be observed in figure 13, the majority of specimens fail at the central zone, and therefore it can be assumed that this failure has been generated under the regularized stress field, whose values are shown in table 9. Replacing these stress components in the considered failure criteria with the allowable of material (X_T = 1746.458 MPa, Y_T = 53.666 MPa, X_C = 1300 MPa, Y_C = 245 MPa) the shear strength S can be evaluated in an indirect way.

In the case of Puck's criterion [55], the failure mode which would be activated is the so-called "inter-fiber failure mode A", whose expression is given by equation (6), where $P_{\perp\parallel}^{(+)}$ is 0.35 for graphite composites, as recommended by the author. The shear strength

value obtained from equation (6), for the stress components corresponding to $\theta = 10^{o}$, is S = 76.819 MPa.

In the case of Tsai-Wu's criterion [54], the expression is given by equation (8). The shear strength value obtained from equation (8), for the stress components corresponding to $\theta = 10^{o}$, is S = 77.887 MPa. As can be observed, the values evaluated by both criteria are very similar, then the average from these values, S = 77.353 MPa, can be taken as representative of the shear strength.

In the case of $\theta = 15^{o}$, as can be seen in figure 14, the majority of specimens fail at a lateral zone near to the end, but at a certain distance from the corner. In order to evaluate the stress field that appears in such zone a FEM model has been developed in commercial code ANSYS [53], consisting of 30150 elements type SHELL63, with 40501 nodes. The mesh (the same used in section 3), as can be seen in figure 5, has been refined conveniently in the area close to the ends to collect the effect of the stress concentration. The discretization has been verified by comparing the results for a mesh with an element size reduced by half, obtaining the same results. To simulate the effect of the non-linear shear behaviour (produced at the failure instant), by means of a linear elastic analysis, the secant shear modulus (G_{12sec} = 2.32 GPa) has been used. As boundary condition, a uniform displacement is applied to produce a longitudinal resultant load F_x = 2970 N, which corresponds to an average stress σ_x = 297 MPa (value of σ_{xu} for $\theta = 15^{o}$).

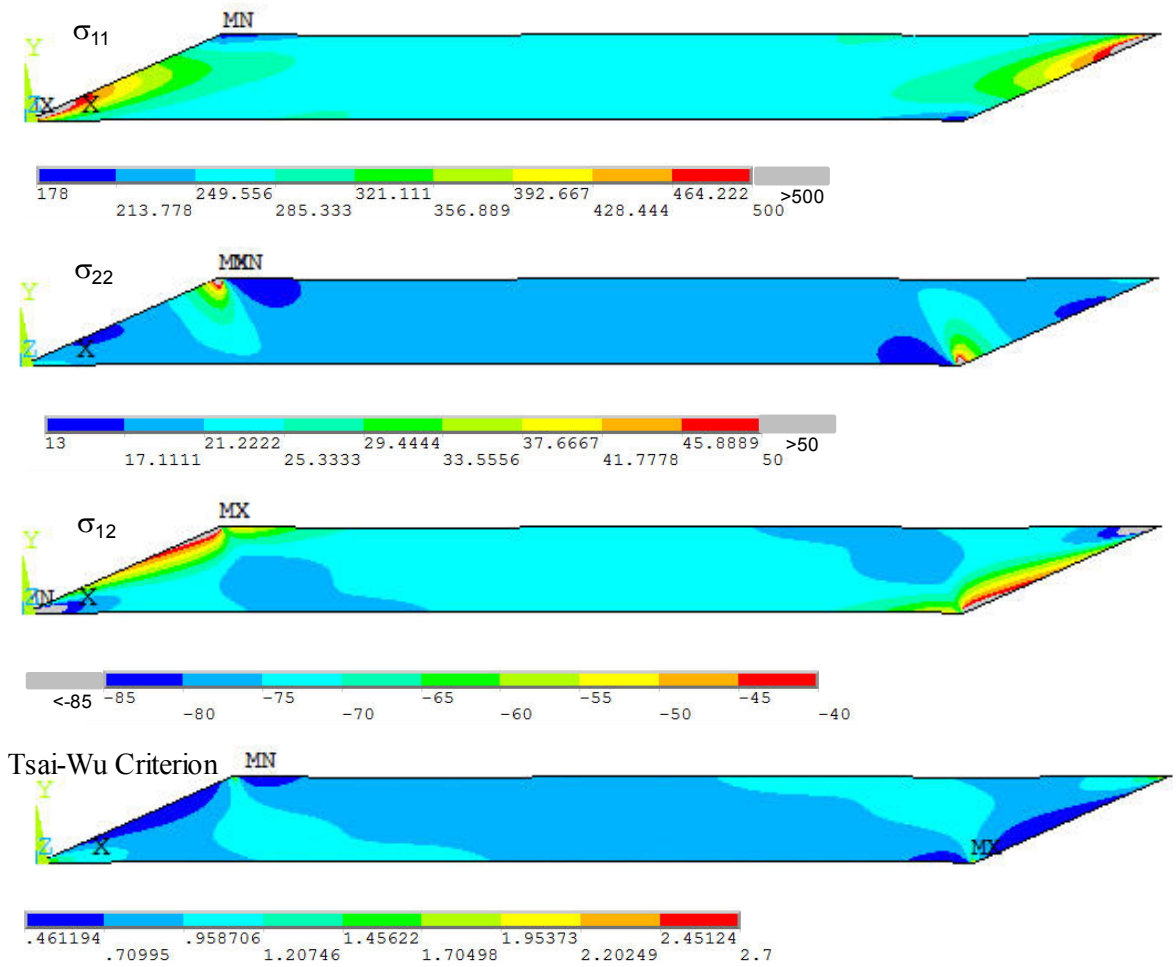

Figure 17.- Numerical results for θ = 15º: stress components σ_1, σ_2, σ_{12}, and value of Tsai-Wu's criterion.

The distribution of stress components (σ_1, σ_2, σ_{12}) in the specimen is shown in figure 17, where a stress concentration (formally a singularity) in σ_2 around the upper corner (left end) can be observed, while σ_{12} presents both a stress concentration (formally a singularity) around the lower corner (left end) and a slight concentration at a certain distance away from the end of specimen. The central zone of specimen is under a uniform stress state, whose values are approximately those showed in table 9 for θ = 15º. Additionally, in figure 17, the value of Tsai-Wu's criterion has been represented, it being observed that a lateral zone (near the extremes of the specimen) appears with values of the criterion higher than one, while in the central zone the values of the

criterion are lesser than one. The values of the criterion achieved in this lateral zone (coloured in light blue in figure 17) are produced by the interaction of both stress components σ_2 and σ_{12}. The failures observed in specimens (see figure 14) at this lateral zone are consequently associated with the high value of the criterion at this zone. Due to the non-uniform stress field observed at this lateral zone, where the failures are located, the shear strength S cannot be evaluated from the measurements of the tests for this fibre orientation.

In the case of $\theta = 20^o$, as can be seen in figure 15, the majority of specimens fail at a lateral zone near to the end, with a similar configuration to the above analysed for $\theta = 15^o$, therefore the explanation made for $\theta = 15^o$ can be extended to interpret the results for $\theta = 20^o$.

Once all considered orientations have been analysed and the 10^o orientation is shown to be the most suitable for test execution, the effect of deviation in tab angle for this orientation ($\theta = 10^o$) has been experimentally studied. For this purpose, from a panel with fibre orientation angle $\theta = 10^o$ six specimens have been obtained, three of those specimens were configured with oblique tabs at $\phi = 25^o$, and in the others three specimens an angle of $\phi = 29^o$ is used for tabs. These tab angles, 25^o and 29^o, produce deviations $\Delta\phi$, with respect to the angle corresponding to $\theta = 10^o$ ($\phi = 22^o$), of $+3^o$ and $+7^o$, respectively. These deviations $\Delta\phi$ have been selected to experimentally check the numerical estimations carried out in previous works [47], which suppose that 3^o deviations could not affect the strength behaviour but 7^o deviations could produce premature failures. The failures observed in specimens of fibre orientation $\theta = 10^o$ for both tab angles $\phi = 25^o$ and $\phi = 29^o$ are shown in figure 18 (a) and (b) respectively.

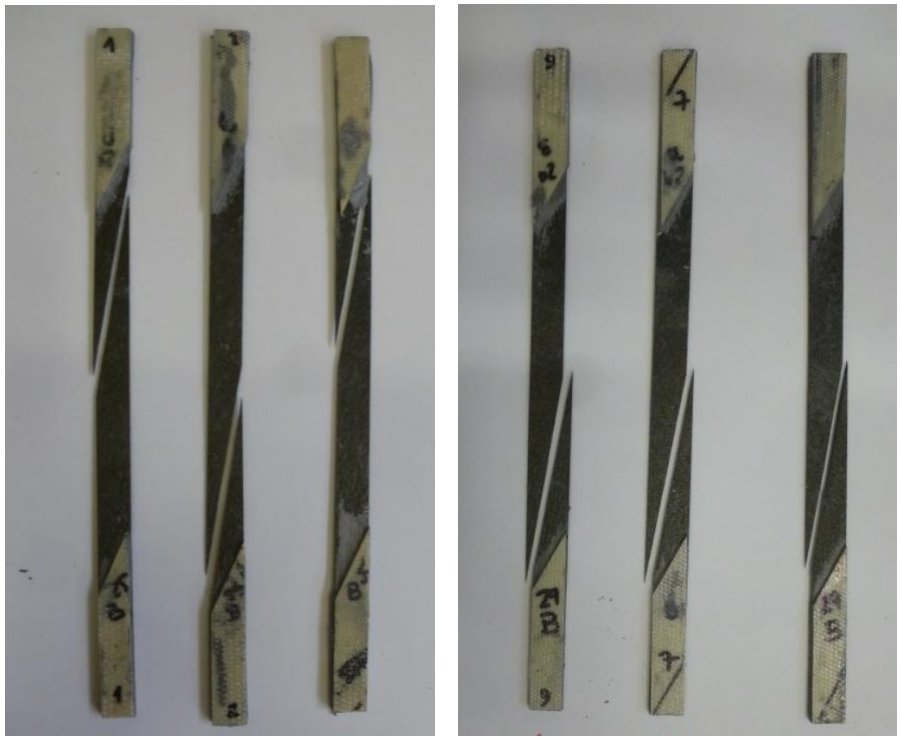

(a) (b)

Figure 18.- View of the failure specimens with fibre orientation $\theta = 10^{o}$ and tab angles: (a) $\phi = 25^{o}$, (b) $\phi = 29^{o}$.

As can be observed in figure 18, in both cases ((a) and (b)) all the failures occur at the ends of specimens, therefore both deviations $+3^{o}$ and $+7^{o}$ generate changes in the stress field around the corner of specimens that increase it severity and produces premature failures. As a consequence, the maximum positive deviation in tab angle must be less than $+3^{o}$ for fibre orientation $\theta = 10^{o}$.

In summary, it would be recommendable to use a tab angle lesser than the theoretic value of ϕ. The reasons behind this recommendation are two:

- Negative deviations in tab angle are favourable in order to decrease the severity of the stress field around the corner of specimen (as can be seen in section 4).
- Positive deviations in tab angle must be avoided because the maximum allowable deviation is lesser than $+3^{o}$.

8. Conclusions.

In the present work, the most adequate fibre orientation angle to perform off-axis tensile tests under an oblique end-tabs configuration is studied. This study is appropriate because, in this configuration, the angle of the tabs depends on both the fibre orientation angle and the properties of the material. For this purpose, an analytical equation for the tab angle ϕ has been obtained, showing that the parameters that ϕ depends on are the fibre orientation angle θ, the quotient G_{12}/E_{11}, the quotient E_{11}/E_{22} and the Poisson's ratio ν_{12}. On the basis of this analytical equation, it is shown that the quotient G_{12}/E_{11} is the most important parameter in the value of the tab angle for a fixed fibre orientation angle. The identification of this main parameter is fundamental to control the deviations in the tab angle due to the uncertainty in the value of the material properties.

Additionally, to study how the deviations in the tab angle affect the stress state at the corners of the specimen, a novel study of the singularity of the nominal stress state at the corner where the failure starts has been developed. The results of this study show that positive deviations in the angle of the tabs ϕ increases the order of the stress singularity, leading to premature failures in the neighbourhood of the corner as is observed in specimens with induced deviations. In contrast, negative deviations in the angle of the tabs ϕ contribute to decrease the severity of the stress state at the corner. From this point of view, as has been shown by this study of stress singularity at the corner of the specimen, the fibre orientation $\theta = 10^{o}$ is optimal in terms of having a tab angle ϕ closest to the angle that would eliminate the singularity ($\delta = 0$).

As has been shown in section 5, a range of suitable fibre orientations θ for the determination of the shear strength S, i.e., those in which the contribution of the shear stress σ_{12} to the failure of the layer is dominant, are located between 5º and 18º. The optimal orientations (where the contribution of σ_{12} to failure is maximal) are located at the lower end of the range, i.e., between 5° and 10°.

In the experimental part of the present work, off-axis tensile tests of graphite-epoxy (AS4/8552) specimens with oblique tabs for four different fibre orientations (5º, 10º, 15º and 20º) have been carried out. Experimental results show that only 10º fibre orientation angle is suitable for the evaluation of shear strength S, because for this orientation the majority of specimens fail at the central zone, the predictions of the study of stress singularities being then confirmed. Thus, for this orientation (θ = 10º) the shear strength S can be evaluated from the regularized stress field by means of a failure criterion. In the present study Puck's and Tsai-Wu's criteria have been used for this purpose obtaining similar values, the average value (77.353MPa) having been taken as representative of the shear strength S value. The other orientations considered (5º, 15º and 20º) fail in the majority of the cases near the extreme of specimen where the stress state is non uniform.

Additionally, for fibre orientation angle θ = 10º, specimens with deviations in tab angle ϕ of +3º and +7º have been tested, it being observed that all the failures appear at the end of specimens. Consequently, deviations in tab angle must be avoided, they having to be lesser than +3º.

In summary, the most suitable fibre orientation angle to perform the off-axis tensile test under oblique end-tabs configuration in graphite-epoxy composites is θ = 10º. Based on

an estimation of material properties (quotient G_{12}/E_{11}) the angle of tabs ϕ can be determined, to use a tab angle lesser than the theoretic one to avoid positive deviations being recommendable.

Acknowledgement

This work was supported by the Spanish Ministry of Education, Culture and Sports under Grant MAT2016-80879-P.

References

1. Floeter L.H. and Boller K.H., Use of experimental rails to evaluate edgewise shear properties of glass-reinforced plastic laminates, U.S. forest products laboratory, Madison, Wisconsin, Task force for test methods, Industry Advisory Group, MIL-HDBK-17, 28 abril 1967.

2. Whitney J.M., Stansbarger D.L., Howell H.B., Analysis of the rail shear test – applications and limitations, J. Composite Materials, 5(1), 1971, pp. 24-34.

3. Hussain A.K., Adams D.F., The Wyoming-modified two-rail shear test fixture for composite materials, J. of Composites Technology and Research, 21(4), 1999, pp. 215-223.

4. Hussain A.K., Adams D.F., Analytical evaluation of the two-rail shear test method for composite materials, Composites Science & Technology, 64(2), 2004, pp. 221-238.

5. Hussain A.K., Adams D.F., Experimental evaluation of the Wyoming-modified two-rail shear test method for composite materials, Experimental Mechanics, 44(4), 2004, pp. 354-364.

6. De Baere I., Van Paepegem W., Degrieck J., Design of a modified three-rail shear test for shear fatigue of composites, Polymer Testing, 27(3), 2008, pp. 346-359.

7. Mohseni Shakib S.M., Li S., Modified three rail shear fixture (ASTM D4255/D 4255M) and an experimental study of non-linear in-plane shear behaviour of FRC, Composites Science & Technology, 69(11-12), 2009, pp. 1854-1866.
8. Whitney J.M., Halpin J.C., Analysis of laminated anisotropic tubes under combined loading, J. Composite Materials, 2, 1968, pp. 360-367.
9. Pagano N.J. and Whitney J.M., Geometric design of composite cylindrical characterization specimens, J. Composite Materials, 4, 1970, pp. 360-378.
10. Pagano N.J. and Halpin J.C., Influence of End Constraint in the Testing of Anisotropic Bodies, J. Composite Materials, 2(1), 1968, pp. 18-31.
11. Wu E.M. and Thomas R.L., Off-axis test of a composite, J. Composite Materials, 2(4), 1968, pp. 523-526.
12. Rizzo R.R., More on the influence of end constraint on off-axis tensile test, J. Composite Materials, 3, 1969, pp. 202-219.
13. Richards G.L., Airhart T.P., Ashton J.E., Off-axis tensile coupon testing, J. Composite Materials, 3, 1969, pp. 586-589.
14. Pipes R.B. and Cole B.W., On the off-axis strength test for anisotropic materials, J. Composite Materials, 7, 1973, pp. 246-256.
15. Chamis C.C. and Sinclair J.H., Ten-deg off-axis test for shear properties in fiber composites, Experimental Mechanics, 17(9), 1977, pp. 339-346.
16. Chang B.W., Huang P.H., Smith D.G., A pinned-end fixture for off-axis testing, Experimental Techniques, 8(6), 1984, pp. 28-30.
17. Pindera M.J. and Herakovich C.T., Shear characterization of unidirectional composites with the off-axis tension test, Experimental Mechanics, 26(1), 1986, pp. 103-112.

18. Cron S.M., Palazotto A.N., Sandhu R.S., The improvement of end-boundary conditions for off-axis tension specimen use, Experimental Mechanics, 28(1), 1988, pp. 14-19.
19. Sun C.T. and Berreth S.P., A new end tab design for off-axis tension test of composite materials, J. Composite Materials, 22(8), 1988, pp. 766-779.
20. Sun C.T. and Chung I., An oblique end-tab design for testing off-axis composite specimens, Composites, 24(8), 1993, pp. 619-623.
21. Marín J.C., Cañas J., París F., Morton J., Determination of G_{12} by means of the off-axis tension test. Part II: A self-consistent approach to the application of correction factors, Composites Part A: applied science and manufacturing, 33(1), 2002, pp. 101-111.
22. Xiao Y., Kawai M., Hatta H., An integrated method for off-axis tension and compression testing of unidirectional composites, J. Composite Materials, 45(6), 2011, pp. 657-669.
23. Petit P.H., A simplified method of determining the in plane shear stress-strain response of unidirectional composites, ASTM STP 460, 1969, pp. 83-93.
24. Rosen B.W., A simple procedure for experimental determination of the longitudinal shear modulus of unidirectional composites, J. Composite Materials, 6(3), 1972, pp. 552-554.
25. Chiao C.C., Moore R.L., Chiao T.T., Measurement of shear properties of fibre composites. Part 1. Evaluation of test methods, Composites, 8(3), 1977, pp. 161-169.
26. Kellas S., Morton J., Jackson K.E., Damage and failure mechanisms in scaled angle-ply laminates, ASTM STP 1156, 1993, pp. 257-280.
27. Arcan M., Hashin Z., Voloshin A., A method to produce uniform plane-stress states with applications to fiber-reinforced materials, Experimental Mechanics, 18(4), 1978, pp. 141-146.

28. Yen S.C., Craddok J.N., Teh K.T., Evaluation of a modified Arcan fixture for the in-plane shear test of materials, Experimental Techniques, 12(12), 1988, pp. 22-25.
29. Hung S.C., Liechti K.M., An evaluation of the Arcan specimen for determining the shear moduli of fiber-reinforced composites, Experimental Mechanics, 37(4), 1997, pp. 460-468.
30. Gan K.W., Laux T., Taher S.T., Dulieu-Barton J.M., Thomsen O.T., A novel fixture for determining the tension/compression-shear failure envelope of multidirectional composite laminates, Composite Structures, 184, 2018, pp. 662-673.
31. Walrath D.E. and Adams D.F., The Iosipescu shear test as applied to composite materials, Experimental Mechanics, 23(1), 1983, pp. 105-110.
32. Adams D.F. and Walrath D.E., Further development of the Iosipescu shear test method, Experimental Mechanics, 27(2), 1987, pp. 113-119.
33. Adams D.F. and Walrath D.E., Current status of the Iosipescu shear test method, J. Composite Materials, 21(6), 1987, pp. 494-507.
34. Prabhakaran R. and Sawyer W., A photoelastic investigation of asymmetric four point bend shear test for composite materials, Composite Structures, 5(3), 1986, pp. 217-231.
35. Inone H., Takanashi M., Nakamura T., Aoki T., Ogasawara T., Modified asymmetric four-point bend test method for in-plane shear properties of ceramic matrix composites at elevated temperatures, Ceramic Engineering and Science Proceedings, 37(2), 2017, pp. 53-60.
36. Sims G.D., Nimmo W., Johnson A.F., Ferriss D.H., Analysis of plate-twist test for in-plane shear modulus of composite materials (revised), Tech. Rep. 54, National Physical Laboratory Report DMM(A), 1994.

37. Gommers B., Verpoest I., Van Houtte P., Further developments in testing and analysis of the plate twist test for in-plane shear modulus measurements, Composites Part A: applied science and manufacturing, 27(11), 1996, pp. 1085-1087.
38. Adams D.O., Moriarty J.M., Gallegos A.M., Adams D.F., Development and evaluation of the V-notched rail shear test for composite laminates, Tech. Rep. Federal Aviation Administration Report DOT/FAA/AR-03/63, FAA Office of Aviation Research, Washington, DC. 2003.
39. Adams D.O., Moriarty J.M., Gallegos A.M., Adams D.F., The V-notched rail shear test, J. Composite Materials, 41(3), 2007, pp. 281-297.
40. Gude M., Hufenbach W., Andrich M., Mertel A., Schirner R., Modified V-notched rail shear test for shear characterisation of textile-reinforced composite materials, Polymer Testing, 43, 2015, pp. 147-153.
41. Mujika F., Valea A., Gañan P., Mondragon I., Off-axis flexure test: a new method for obtaining in-plane shear properties, J. Composite Materials, 39(11), 2005, pp. 953-980.
42. Vargas G., Mujika F., Determination of in-plane shear strength of unidirectional composite materials using the off-axis three-point flexure and off-axis tensile tests, J. Composite Materials, 44(21), 2010, pp. 2487-2507.
43. Cabrero J.M., Vargas G., Analysis of the validity of the three-point off-axis bending method, Applied Mathematical Modelling, 39, 2015, pp. 5265-5277.
44. Trappe V., Basan R., Grasse F., Stiffness and fracture of shear loaded laminates with unidirectional and biaxial fibre orientation investigated with a picture frame test, 16th European Conference on Composite Materials, ECCM16, 2014.

45. Pierron, F.; Vautrin, A., "10° off-axis tensile test: A critical approach", Composites Science and Technology, v56, n4, p 483-488, Apr 1996.

46. Kawai, M.; Morishita, M.; Satoh, H.; Tomura, S.; Kemmochi, K., "Effects of end-tab shape on strain field of unidirectional carbon/epoxy composite specimens subjected to off-axis tension", Composites - Part A: Applied Science and Manufacturing, v 28, n 3, p 267-275, 1997.

47. Pierron, F.; Alloba, E.; Surrel, Y.; Vautrin, A., "Whole-field assessment of the effects of boundary conditions on the strain field in off-axis tensile testing of unidirectional composites", Composites Science and Technology ,v 58, n 12, p 1939-1947, Dec 1998.

48. Pierron, F.; Vautrin, A., "New ideas on the measurement of the in-plane shear strength of unidirectional composites", Journal of Composites Materials, v 31, n 9, p 889-895, 1997.

49. Tsai S. W., Composites Design, Think Composites, 1988.

50. MIL-HDBK-17-2E, Polymer Matrix Composites. Materials Propierties, Department of Defense Handbook, 1998.

51. Schwartz M. M., Composite Materials Handbook, Mc Graw-Hill Book Company, 1984.

52. Herakovich C. T., Mechanics of Fibrous Composites, John Wiley & Sons, Inc., 1998.

53. ANSYS. Swanson Analysis System, Inc.; 2011.

54. Tsai, S.W. and Wu, E.M., "A general theory of strength for anisotropic materials", J. Compos. Mater., vol. 5, pp. 58-80, 1971.

55. Puck, A. and Schurmann, H., "Failure analysis of frp laminates by means of physically based phenomenological models", Composites Science and Technology, vol.58(7), pp. 1045-1067, 1998.

56. Barroso A. Mantic, V, París, F. Singularity analysis of anisotropic multimaterial corners. International Journal of Fracture 119, pp.1-23, 2003.

57. Mantic, V, Barroso, A, París, F. Singular elastic solutions in anisotropic multimaterial corners. Application to composites. Chapter 11 of the book “Mathematical methods and models in composites”, Edited by Mantic, V. Imperial College Press, pp:425-495, 2014.

58. Odegard, G.; Kumosa, M., "Determination of shear strength of unidirectional composite materials with the iosipescu and 10º off-axis shear tests", Composites Science and Technology, vol.60(16), p 2917-2943, 2000.

59. Odegard, G.; Kumosa, M., "Elastic-plastic and failure properties of a unidirectional carbon/PMR-15 composite at room and elevated temperatures", Composites Science and Technology, vol.60(16), p 2979-2988, 2000.

60. Xavier J.C., Garrido N.M., Oliveira M., Morais J.L., Camanho P.P., Pierron F., A comparison between the Iosipescu and off-axis shear test methods for the characterization of Pinus Pinaster Ait, Composites Part A: applied science and manufacturing, 35A (7-8), pp. 827-840, 2004.

61. Hinton, M.J., Kaddour, A.S. Soden, P.D.,, "A comparison of the predictive capabilities of current failure theories for composite laminates, judged against experimental evidence", Composites Science and Technology, vol.62(12-13), p 1725-1797, 2002.

62. Liu, K.-S., Tsai S.W., "A progressive quadratic failure criterion for a laminate", Composites Science and Technology, vol.58(7), pp. 1023-1032, 1998.